2D NUMERICAL MODELING OF NATURALLY FRACTURED MEDIA USING FINITE ELEMENTS WITH HIGH ASPECT RATIO

Pedro R. Cleto

Osvaldo L. Manzoli

Heber A. A. Fabbri

Eduardo A. Rodrigues

José H. K. Ambiel

pedro.cleto@feb.unesp.com

omanzoli@feb.unesp.br

heber.fabbri@feb.unesp.br

eduardoalex@feb.unesp.br

zeambiel@hotmail.com

Mechanical Engineering Department - São Paulo State University - UNESP

Avenida Engenheiro Luiz Edmundo Carrijo Coube 14-01, 17033-360, Bauru, São Paulo, Brasil

Abstract. *Many reservoirs are naturally fractured presenting several pre-existing fractures that can form complex networks. When the fluid pressure decreases within a fracture, a reduction of its opening occurs due to the increase of the effective stresses. Seeking to better understand the influence of natural fractures permeability on pressure field and fluid flow in the reservoir, this work proposes a 2D finite element approach to model the fracture closure in naturally fractured reservoirs, which are explicitly represented by finite elements with high aspect ratio. A novel constitutive model based on concepts of damage mechanics and the nonlinear Barton-Bandis joint mechanical model is used to model the fracture closure. The fluid flow is described by Darcy's law and one-way coupling method is used to solve the hydromechanical equations. Numerical examples with different fracture geometries are conducted to show the efficiency and accuracy of the employed model. The results show that the proposed model is able to reproduce the effects of the changing fracture permeability on pressure field and fluid flow in the reservoir.*

Keywords: *Natural fractures, Elements with high aspect ratio, Barton-Bandis joint model, Hydromechanical analysis*

CILAMCE 2017
Proceedings of the XXXVIII Iberian Latin-American Congress on Computational Methods in Engineering
P.O. Faria, R.H. Lopez, L.F.F. Miguel, W.J.S. Gomes, M. Noronha (Editors), ABMEC, Florianópolis, SC, Brazil, November 5-8, 2017

1 INTRODUCTION

Naturally fractured reservoirs are media composed of two mediums with distinct properties: rock matrix and fractures (Abdelazim and Rahman, 2016). According to Weng (2015), in general, the fluid flow simulation in reservoirs containing a large number of natural fractures has been performed according to two approaches: the first based on the continuous approach, which represents a heterogeneous reservoir with natural fractures as an equivalent homogeneous medium; and the second based on the discrete fracture network (DFN), which explicit considers the natural fractures of the reservoir, taking into account the size, shape and distribution of them, as well as their flow properties.

Abdelazim and Rahman (2016) states that fractures are discontinuities that affect both the mechanical stability and the fluid flow of the reservoir, and therefore, for an appropriate estimation of the production potential and selection of production methods, it is essential to properly understand the fluid flow behavior on fractures network.

This work aim to present a novel tool for hydromechanical behavior modeling and simulation of naturally fractured reservoirs subject to depressurizing. Natural fractures are explicitly represented by finite elements with high aspect ratio (Manzoli et al., 2012, 2014; Sánchez et al., 2014; Manzoli et al., 2016) using a constitutive model based on the closure model proposed by Barton et al. (1985).

1.1 Barton-Bandis joint mechanical model

By studying the hydromechanical behavior of fractured rocks by means of laboratory tests, Barton et al. (1985) verified that the normal strains to the plane of the fracture (closure) and the strains by shear (dilatancy) can significantly modify the hydraulic conductivity of the fracture. This occurs due to the fact that its opening (both mechanical and hydraulic) may vary depending on the normal compressive stress or by shear expansion. When the fractured rock is submitted to depressurizing the compression (in terms of effective stresses) increases and the corresponding fracture strain, becomes the key variable to represent its hydraulic behavior, since the fracture permeability directly depends on its opening.

Barton et al. (1985) presented a hyperbolic model for the relationship between fracture compression normal stress and normal strain, based on experimental results, describing this type of problem by a closure-stress relationship in which the fracture normal stiffness, K_{ni}, and normal closure, ΔV_j, are considered explicitly according to the relation:

$$\sigma_n = \frac{K_{ni} V_m \Delta V_j}{V_m - \Delta V_j}, \tag{1}$$

where σ_n is the compression normal stress and V_m is the fracture maximum closure.

2 GOVERNING EQUATIONS

2.1 Equations of conservation

Consider an arbitrary volume control crossed for a single-phase fluid flow and a saturated porous media. The equation of conservation of fluid mass can be written as:

$$\frac{\partial}{\partial t}\left(\phi \rho_f\right) + \boldsymbol{\nabla} \cdot \mathbf{j}_{\boldsymbol{f}} = 0, \tag{2}$$

where ϕ is the porosity of the rock ($0 \leq \phi < 1$), ρ_f is the fluid density and $\mathbf{j_f}$ is the fluid mass flow vector.

The storage term of Eq. (2) is responsible to transient part and, for sake of simplicity, it was neglected. The transport term of Eq. (2), which corresponds to the steady state, is given by

$$\mathbf{j_f} = \rho_f \mathbf{q_f}, \tag{3}$$

where $\mathbf{q_f}$ is the fluid flux given by Darcy's Law, which is applied to laminar flows of Newtonian fluids in porous media. Considering the flow direction perpendicular to the gravity and an isotropic medium, the Darcy's expression can be written as:

$$\mathbf{q_f} = -\frac{k}{\mu_f} \boldsymbol{\nabla} p_f, \tag{4}$$

where k is the intrinsic permeability of the rock, μ_f is the dynamic viscosity of the fluid and p_f is the porepressure.

In addition to the Eq. (2) the equation of conservation of solid mass is written as

$$\frac{\partial}{\partial t} \left[(1-\phi)\, \rho_s \right] + \boldsymbol{\nabla} \cdot \left[(1-\phi)\, \rho_s \dot{\mathbf{u}} \right] = 0, \tag{5}$$

where ρ_s is the solid density and $\dot{\mathbf{u}}$ is the displacement velocity vector of the solid.

From Eq. (5), applying the concept of material derivative and considering an incompressible medium, the porosity of the rock is given by (Guimarães, 2002):

$$\phi = 1 - (1 - \phi_0)^{\epsilon_v}. \tag{6}$$

where ϕ_0 is the initial porosity of the rock and ϵ_v is the volumetric strain.

Finally, the permeability of the rock can be calculated according to well-known Kozeny-Carman's model, given by:

$$k = k_0 \frac{\phi^3}{(1-\phi)^2} \frac{(1-\phi_0)^2}{\phi_0^3}, \tag{7}$$

where k_0 is the initial intrinsic permeability of the rock.

2.2 Balance equation with hydromechanical coupling

According to the Terzaghi's Effective Stress Principle (Terzaghi, 1943), the total stress in a porous medium is related with porepressure as:

$$\boldsymbol{\sigma} = \boldsymbol{\sigma'} + p_f \mathbf{I}, \tag{8}$$

where $\boldsymbol{\sigma'}$ is the Terzaghi's effective stresses tensor and $\mathbf{I}$ is the second order unit tensor. Note that effective stress tends to increase according to decreasing poropressure.

The Terzaghi's effective stresses tensor is written in terms of the strains via a constitutive relationship, $\Sigma(\cdot)$, as follows:

$$\boldsymbol{\sigma'} = \Sigma\left(\boldsymbol{\epsilon}\right), \tag{9}$$

where $\boldsymbol{\epsilon}$ is the strain tensor.

3 SOLID FINITE ELEMENT WITH HIGH ASPECT RATIO

Consider a three nodes solid finite element with base b, which is defined by the distance between the nodes 2 and 3, and height h, which is defined by the distance between the node 1 and its projection on the base $1'$, as shown in Fig. 1. When $h \to 0$ this kind of element present a high aspect ratio (ratio of the largest to the smallest dimension) given by $^b/_h$ (see Fig. 1).

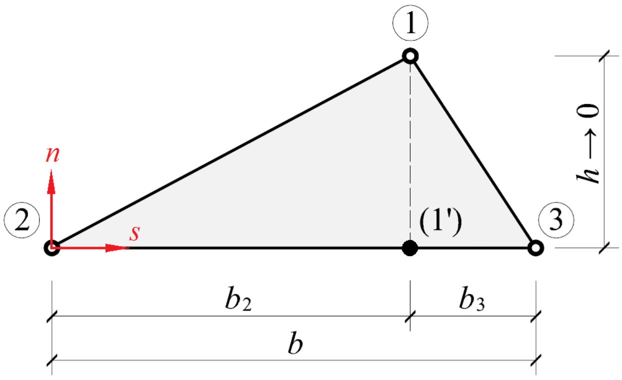

Figure 1: Three nodes solid finite element with high aspect ratio (adapted from Manzoli et al. (2012)).

Consider also $b_2 = \alpha b$ and $b_3 = (1 - \alpha)\, b$, where $0 \leqslant \alpha \leqslant 1$ is a multiplier factor. Thus:

$$\begin{cases} \mathbf{x}^{(1)} = (\alpha b, h) \\ \mathbf{x}^{(2)} = (0, 0) \\ \mathbf{x}^{(3)} = (b, 0) \end{cases}, \tag{10}$$

where $\mathbf{x}^{(1)}$, $\mathbf{x}^{(2)}$ and $\mathbf{x}^{(3)}$ are the Cartesian coordinates of the nodes 1, 2 and 3, respectively.

3.1 Hydraulic formulation

Considering the reference system (n, s), which is presented in the Fig. 1, the gradient of the pressure field approximation in the element is given by (Seixas, 2015; Cleto, 2016):

$$\boldsymbol{\nabla} p_f = \left\{ \begin{array}{c} \dfrac{1}{b}\left(p^{(3)} - p^{(2)}\right) \\ \dfrac{1}{h}[\![p]\!] \end{array} \right\}, \tag{11}$$

where $[\![p]\!] = p^{(1)} - \left[(1-\alpha)\, p^{(2)} + \alpha p^{(3)}\right] = p^{(1)} - p^{(1')}$ and $p^{(1)}$, $p^{(2)}$ and $p^{(3)}$ are the pressures on the nodes 1, 2 and 3, respectively (see Fig. 1). Note that $[\![p]\!]$ is the pressure jump and it corresponds to the difference of pressure between the node (1) and its projection on the base of the element $(1')$.

According to Darcy's Law, the flow within the element is given by:

$$\mathbf{q}_f = \tilde{\mathbf{q}}_f + \hat{\mathbf{q}}_f = -\frac{k}{b\,\mu_f} \left\{ \begin{array}{c} p^{(3)} - p^{(2)} \\ 0 \end{array} \right\} - \frac{k}{h\,\mu_f} \left\{ \begin{array}{c} 0 \\ [\![p]\!] \end{array} \right\}. \tag{12}$$

Note that there are two parts that define the flow: the first one, $\tilde{\mathbf{q}}_f$, depends on the base b; and the second one, $\hat{\mathbf{q}}_f$, depends on the height h. In the limit situation of $h \to 0$, the flow in the interface element must remain bounded. Therefore, in this case, the pressure jump must tend to zero ($[\![p]\!] \to 0$), which means that the pressure on the node (1) and its projection on the base $(1')$ tends to the same value.

Note that the first component of the flux in $\tilde{\mathbf{q}}_f$ is proportional to the difference between the nodal pressure of the nodes 3 and 2, respectively. As a consequence, the solid element acts as a one-dimensional element conducting the flux along the interface element.

The description of the mechanical behavior of the elements with high aspect ratio can be found in the works from Manzoli et al. (2012), Manzoli et al. (2014) and Manzoli et al. (2016).

3.2 Mesh fragmentation technique

Figure 2 illustrates the mesh fragmentation technique and insertion of elements with high aspect ratio (or, for simply, interface elements) (Manzoli et al., 2014; Sánchez et al., 2014; Manzoli et al., 2016). Basically, the mesh fragmentation technique consists on 3 steps: (1) choose a interest region of the mesh (Fig. 2a); (2) decrease the size of the regular finite elements (Fig. 2b); (3) accommodate a couple of triangular interface elements (Fig. 2c).

Once the domain of the sample to be studied is defined, for the two-dimensional case, the natural fractures are inserted into the geometry of the domain as straight lines which may or not intersect each other. Thus, knowing the position of each natural fracture and using a specific *in house* algorithm, those interface elements that were positioned exactly on the natural fractures has a exclusive constitutive model and properties. In this work, a novel model based on nonlinear Barton-Bandis joint mechanical model is assigned to the interface elements that represent natural fractures while a linear elastic model is assigned to the regular elements.

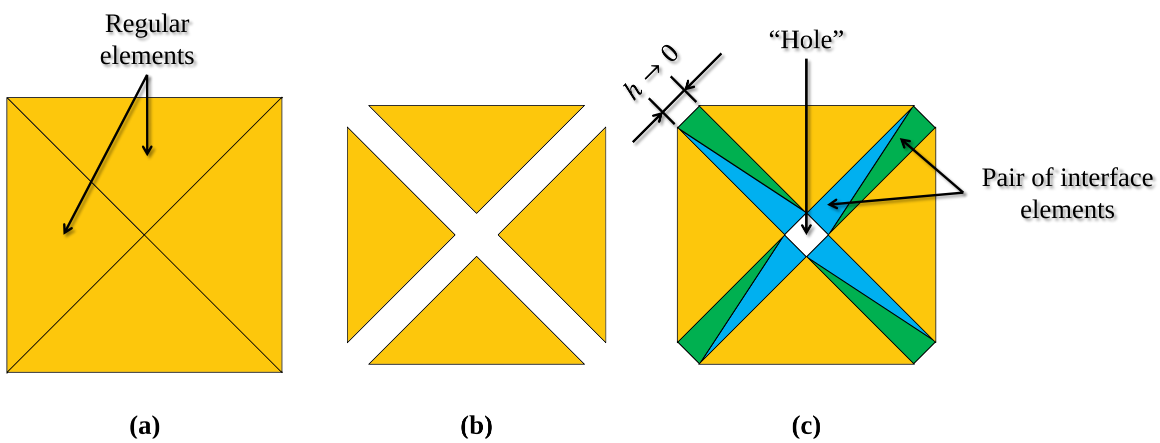

Figure 2: Mesh fragmentation technique (adapted from Cleto (2016)). (a) Original mesh with regular elements. (b) Reduction of the size of the regular elements. (c) Accommodation of the interface elements.

As a consequence of this technique, "holes" (spaces without any properties) appear throughout the mesh causing influence on flux (Eq. (12)). To avoid this influence, the pressures on nodes 1 and 3 are forced to be equal via a penalty technique (see Fig. 1).

3.3 Fracture permeability variation law

The parallel plates model is a simple way to describe the fluid flow confined within a fracture formed by two smooth plates separated by an aperture a_{fr}. Neglecting imperfections in the walls of the fracture, like roughness, and considering a laminar flow with parabolic velocity distribution in the cross section of fracture, the permeability of the fracture k_{fr} is given by (Snow, 1965):

$$k_{fr} = \frac{a_{fr}^2}{12} = \frac{(a_0 + [\![u]\!]_n)^2}{12}, \tag{13}$$

where a_0 is the initial aperture of the natural fracture and $[\![u]\!]_n$ is the normal component of the displacement jump (Manzoli et al., 2012, 2014, 2016), which corresponds to the variation of fracture opening.

4 CONTINUUM CONSTITUTIVE MODEL

The closure model proposed in this work is applicable only in cases of compression. It is based on the tension damage model present by Manzoli et al. (2014) and the constitutive model of joint behavior present by Barton et al. (1985).

To describe the fracture closure model, consider, firstly, the continuum model given by following constitutive relation:

$$\boldsymbol{\sigma'} = \Sigma\left(\boldsymbol{\epsilon}\right) \Rightarrow \boldsymbol{\sigma'} = \xi\, \bar{\boldsymbol{\sigma}} \Rightarrow \boldsymbol{\sigma'} = \xi\, \mathbb{C} : \boldsymbol{\epsilon}\,, \tag{14}$$

where $\boldsymbol{\sigma'}$ is the Terzaghi's effective stress tensor, ξ is a "contact" internal variable which increases according to fracture closure ($0 \leqslant \xi \leqslant 1$), $\bar{\boldsymbol{\sigma}}$ is the elastic stress tensor and $\mathbb{C}$ is the fourth order elastic constitutive tensor.

The contact criterion defines the elastic domain and it is based on the component of the Terzaghi's effective stress tensor normal to the base of the interface element (σ'_{nn}), given by

$$\varphi = -\sigma'_{nn} + r(\bar{r}) \leqslant 0, \tag{15}$$

where $\sigma'_{nn} = \mathbf{n} \cdot \boldsymbol{\sigma'} \cdot \mathbf{n}$, $\mathbf{n}$ is the normal vector to the base of the interface element and r and $\bar{r}$ are stress and strain-like internal variables, respectively.

The contact criterion can be expressed in terms of elastic stresses dividing the Eq. (15) by ξ. Thereby, Eq. (15) is rewritten as:

$$\bar{\varphi} = -\bar{\sigma}_{nn} + \bar{r} \leqslant 0, \tag{16}$$

with

$$\bar{r} = \frac{r}{\xi} \tag{17}$$

and

$$\bar{\sigma}_{nn} = \frac{\sigma'_{nn}}{\xi}. \tag{18}$$

Note that $\bar{r}$ controls the size of the elastic domain in the space of the elastic stress. Thus, the contact evolution law can be written in terms of internal variable $\bar{r}$, as:

$$\xi(\bar{r}) = \frac{r(\bar{r})}{\bar{r}}. \tag{19}$$

The evolution law for the strain-like internal variable along the loading process time t is given by:

$$\bar{r}(t) = \bar{r}_t = \max_{s\in[0,t]}[-\bar{\sigma}_{nn}(s), 0]. \tag{20}$$

During the loading process, the contact internal variable ($\bar{r}$) starts with 0 (zero) and assumes the maximum compression stress value that the elastic stress tensor component $\bar{\sigma}_{nn}$ reaches.

Finally, adapting the model proposed by Barton et al. (1985) (Eq. (1)) to the contact model described, the evolution of the r variable is express by means of the following law:

$$r(\bar{r}) = \frac{K_{ni}V_m}{\left(\dfrac{V_m E}{h} - \bar{r}\right)}\,\bar{r}, \tag{21}$$

where E is the Young's modulus of the rock.

For integration of the contact model, an implicit-explicit (IMPL-EX) integration algorithm (proposed by Oliver et al. (2006)) is used as detailed in Manzoli et al. (2016).

5 NUMERICAL EXAMPLES

The proposed examples aim to evaluate if interface elements are able to represent the fracture closure effect according to the rock porepressure variation. For this, the simulations were performed in the context of small deformations and considering the plane strain. With respect to the interface elements, a thickness of $h = 0.0001$ m was attributed.

Three regions of 100.0×100.0 m with different densities of natural fractures oriented horizontally and vertically were analyzed. For all natural fractures an initial aperture (a_0) of 3.0×10^{-5} m was assumed. Furthermore, according to the Barton's joint closure model, $K_{ni} = 1.0 \times 10^4$ MPa/m and $V_m = 3.0 \times 10^{-5}$ m also was attributed to the natural fractures. Note that the maximum closure of the fractures was assumed as the initial aperture.

Figure 3 shows the three finite element meshes were used. The first one has a low number of natural fractures (Fig. 3a and will be treated as "Region 1"; the second one has an intermediate number of natural fractures (Fig. 3b) and will be treated as "Region 2"; the third one presents a high number of natural fractures (Fig. 3c) and will be treated as "Region 3". Note that the red lines highlight the position of the natural fractures in each mesh. Only linear triangular elements were used in all meshes.

Table 1 presents the mechanical and hydraulical properties of the rock and Table 2 presents the fluid properties.

The boundary conditions are shown in Fig. 4. *In situ* stresses are imposed in the first loading interval, which correspond to 50.00 MPa (Fig. 4a). In the second loading interval, pressures

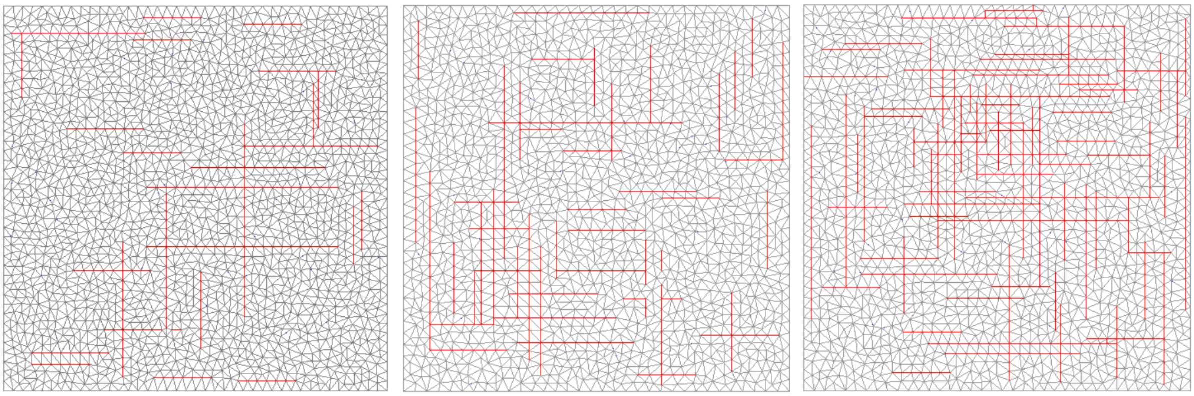

(a) (b) (c)

Figure 3: Finite element mesh highlighting the natural fractures position. (a) Region 1: low fractures density. (b) Region 2: intermediate fractures density. (c) Region 3: high fractures density.

Table 1: Mechanical and hydraulical properties of the rock

Propertie	Nomenclature	Value
Young's modulus (MPa)	E	16.9
Poisson's ratio (-)	ν	0.3
Initial intrinsic permeability (m^2)	k_0	1.0×10^{-17}
Initial porosity (-)	ϕ_0	0.1

of 45.00 MPa and 44.90 MPa, 39.95 MPa and 39.85 MPa and 4.85 MPa and 4.75 MPa are imposed on opposite sides of the domain (Fig. 4b). Thus, as a consequence of reduction of the porepressure, the compression effective stress increases causing the fracture closure.

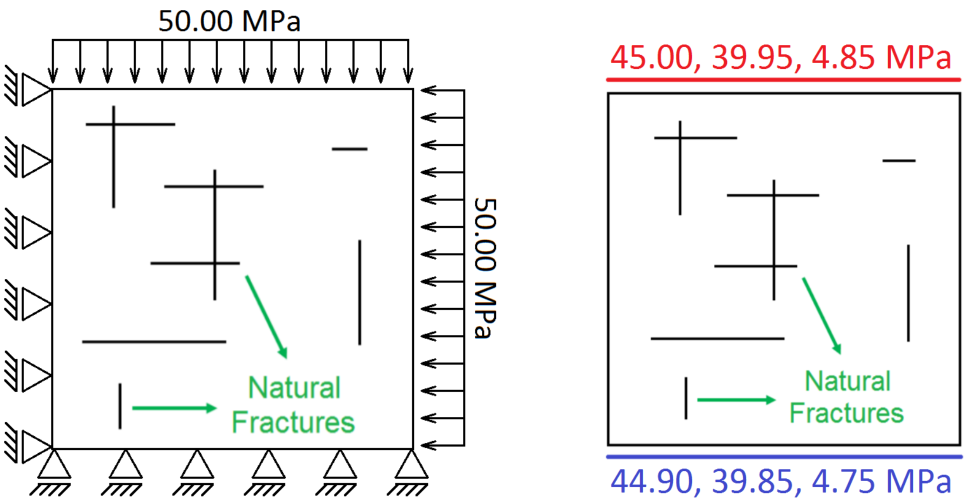

(a) (b)

Figure 4: Boundary conditions. (a) Initial loading to confine the domain. (b) Pressure variation keeping a difference of 0.1 MPa.

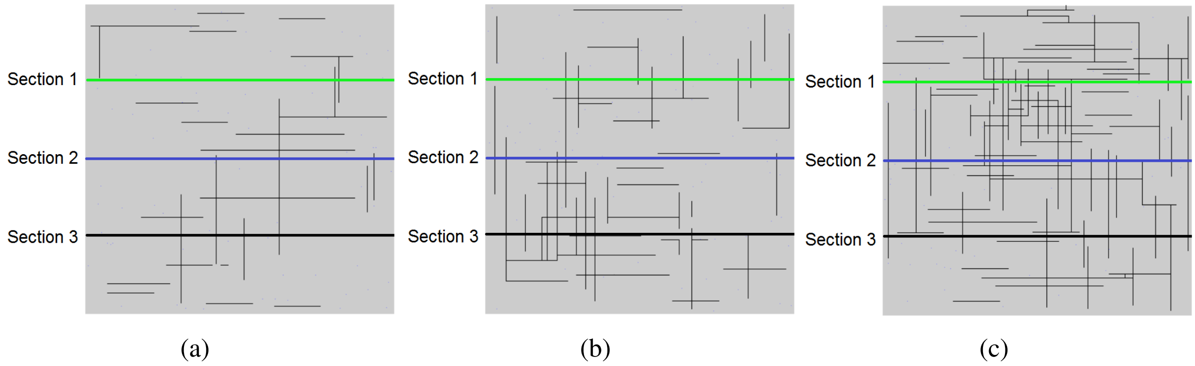

Figure 5: Cross section lines. (a) Region 1. (b) Region 2. (c) Region 3.

The pressure cross section shown in the following results was obtained at three different heights as can be seen in Fig. 5: 75.0 m (indicated by "Section 1"), 50.0 m (indicated by "Section 2") and 25.0 m (indicated by "Section 3").

Table 2: Fluid properties

Propertie	Nomenclature	Value
Dynamic viscosity (MPa s)	μ_f	1.0×10^{-9}
Density ($\mathrm{kg/m^3}$)	ρ_f	1002.6

Figure 6 shows the pressure field and its pressure cross section for these three different pressure pairs applied on boundary (45.00 to 44.90 MPa, 39.95 to 39.85 MPa and 4.85 to 4.75 MPa) considering the Region 1. Note that pressure field tends to remain constant along the natural fractures, because their permeability is much greater than rock. Note also that decreasing applied pressure, the field tends to become uniform. This occurs due to the fractures closure, which results in a decrease of its permeability according to Eq. (13).

Figure 7 shows the pressure field and its pressure cross section for these three different pressure pairs applied on boundary (45.00 to 44.90 MPa, 39.95 to 39.85 MPa and 4.85 to 4.75 MPa) considering the Region 2. Note that effect of natural fractures on pressure field is similar to the previously described.

Figure 8 shows the pressure field and its pressure cross section for these three different pressure pairs applied on boundary (45.00 to 44.90 MPa, 39.95 to 39.85 MPa and 4.85 to 4.75 MPa) considering the Region 3. As in the cases described previously, natural fractures affect the pressure field due to its high permeability, but increasing the effective stresses with a consequent reduction of the fractures aperture, this effect on pressure field becomes negligible.

Another result obtained was the equivalent permeability of the considered 3 regions according to the imposed pressures, which are presented in Table 3. Each permeability was calculated from the nodal rate flows using Darcy's Law.

Note that the equivalent permeabilities present, in general, higher values than that assigned to rock (see Table 1) where a expressive increase can be seen on Region 3 (high density of natural fractures). This occurs due to the influence of natural fractures, which are much more

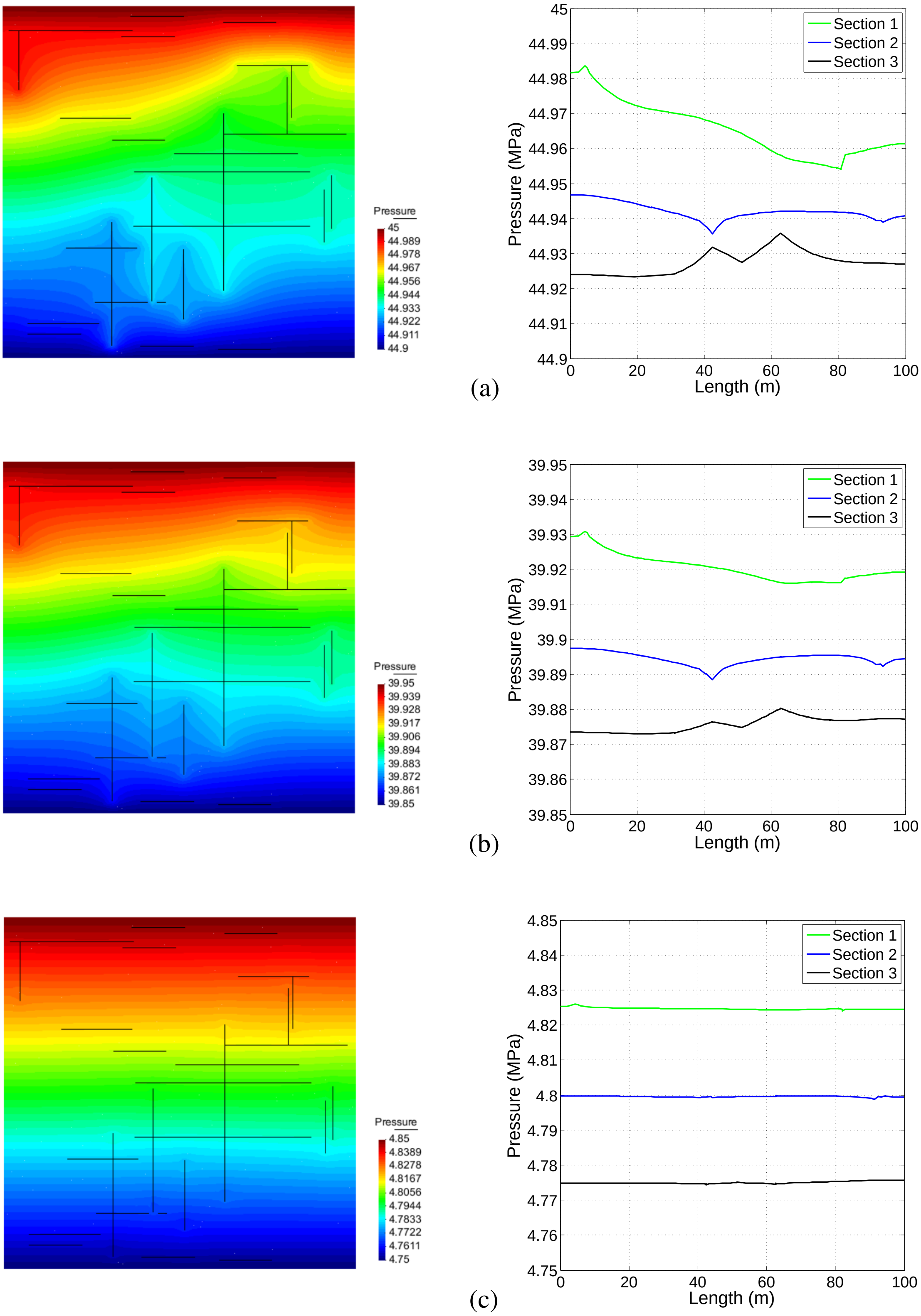

Figure 6: Pressure field and corresponding pressure cross section of the Region 1 considering pressures of (a) 45.00 MPa and 44.90 MPa, (b) 39.95 MPa and 39.85 MPa and (c) 4.85 MPa and 4.75 MPa.

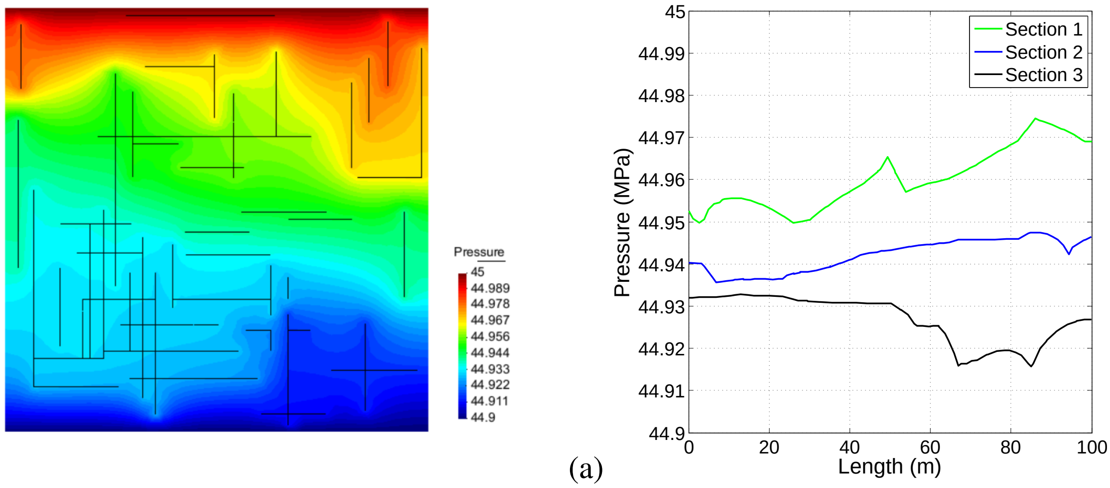

(a)

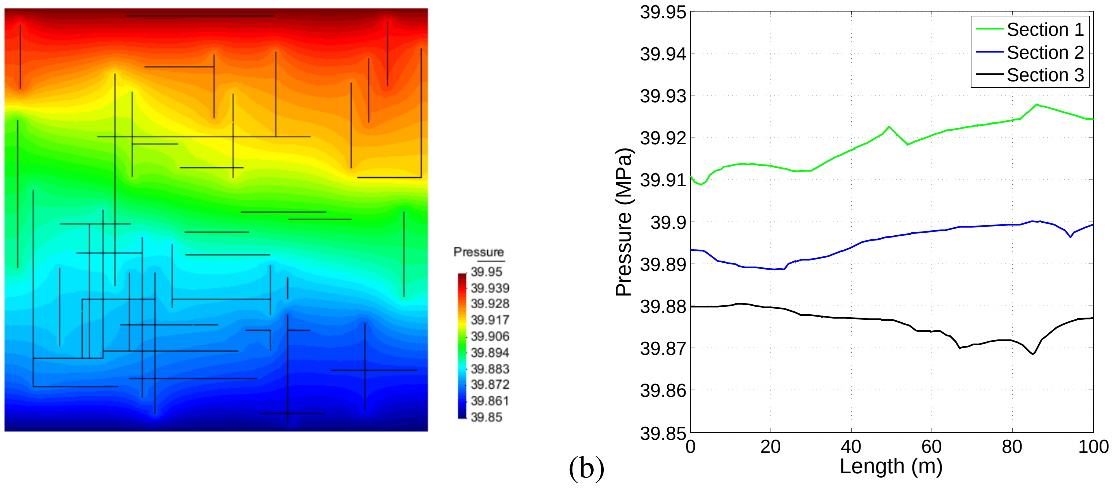

(b)

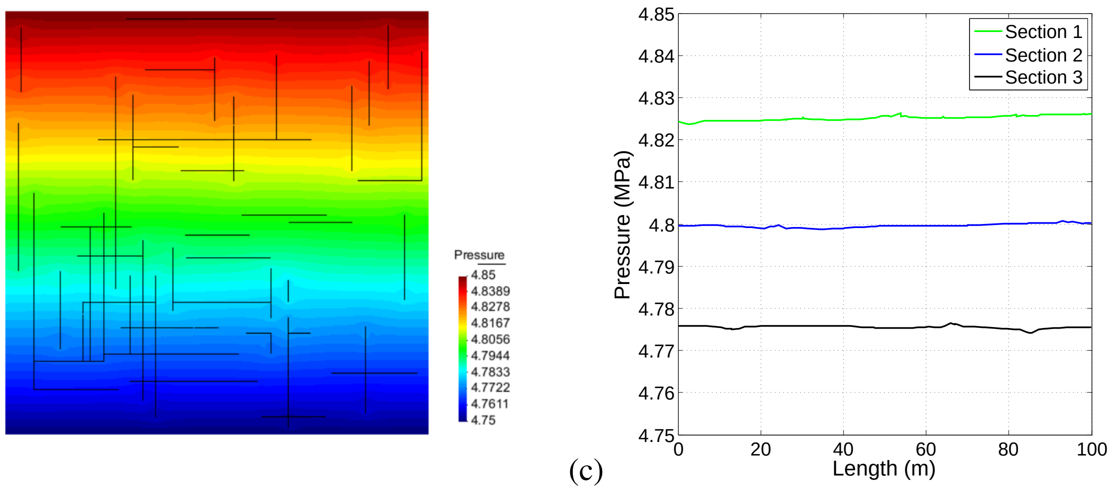

(c)

Figure 7: Pressure field and corresponding pressure cross section of the Region 2 considering pressures of (a) 45.00 MPa and 44.90 MPa, (b) 39.95 MPa and 39.85 MPa and (c) 4.85 MPa and 4.75 MPa.

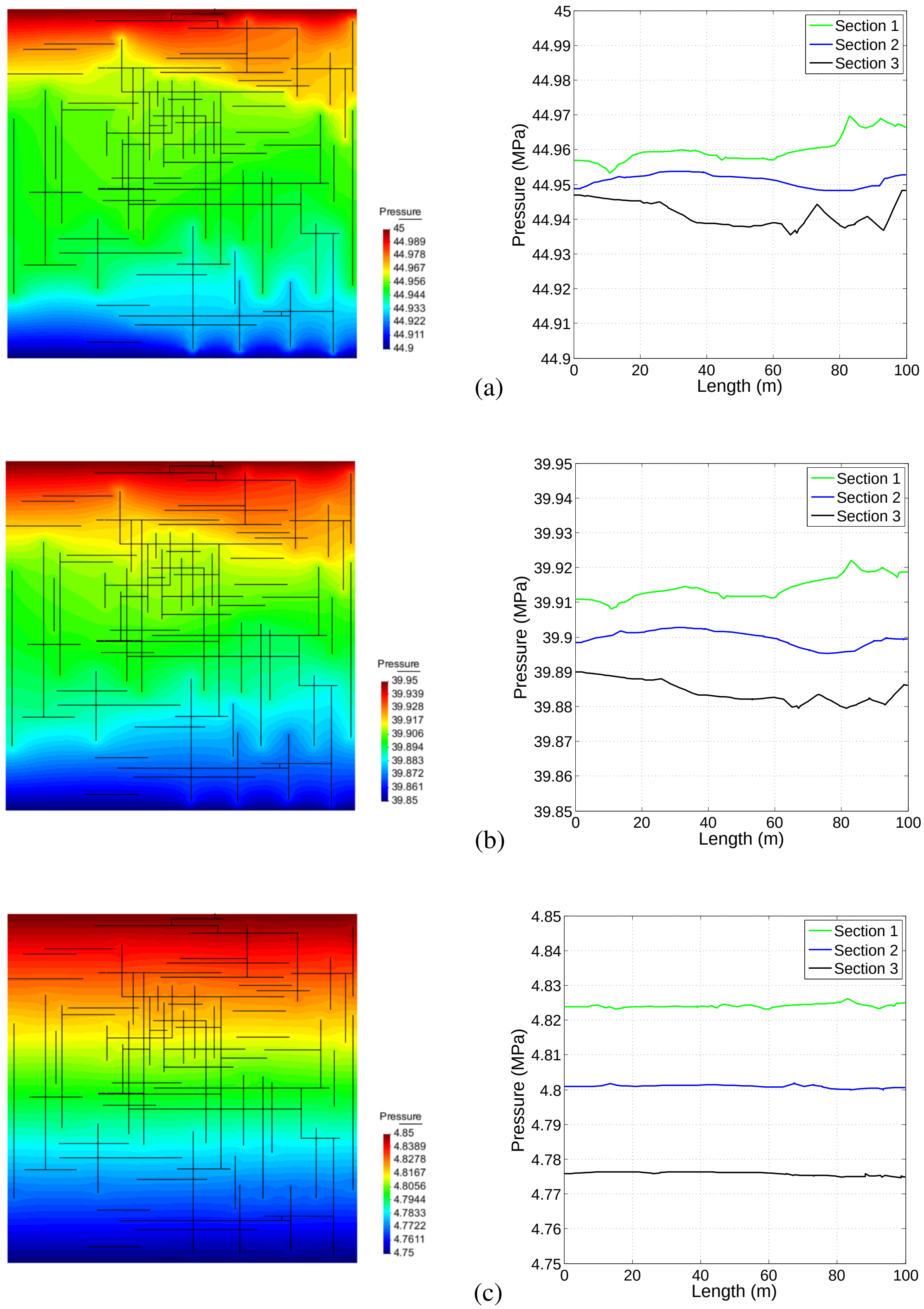

Figure 8: Pressure field and corresponding pressure cross section of the Region 3 considering pressures of (a) 45.00 MPa and 44.90 MPa, (b) 39.95 MPa and 39.85 MPa and (c) 4.85 MPa and 4.75 MPa.

permeable than rock. Once the fractures are submitted to a permeability variation by decreasing the porepressure, according to Eq. (13), the equivalent permeability also decreases, evidencing the closure of the natural fractures.

Table 3: Equivalent permeabilities

		Region		
		1	**2**	**3**
Boundary pressure (MPa)	**45.00 to 44.90**	1.72×10^{-17}	2.73×10^{-17}	4.48×10^{-17}
	39.95 to 39.85	1.36×10^{-17}	1.92×10^{-17}	2.56×10^{-17}
	4.85 to 4.75	0.96×10^{-17}	1.02×10^{-17}	1.04×10^{-17}

In addition, for the Region 1 and porepressures of 4.85 to 4.75 MPa, the equivalent permeability is lower than that assigned to rock (see Table 1). This effect occurs due to compression effective stresses which cause a rock permeability decrease according to Eq. (7).

6 CONCLUSIONS

This work presented a new approach to simulate the fracture closure in naturally fractured reservoirs. A novel method based on nonlinear Barton-Bandis joint model was used to relate the normal stress and strain on fracture plane. By means of a hydromechanically coupled finite element formulation, special elements with a high aspect ratio (interface elements) was used to represent the natural fractures. They were able to work as a very permeable channel transmitting the pressure along the fractures and its eventual connections.

The proposed contact model allied to the mesh fragmentation technique using interface elements showed to be very promising for the modeling and simulation of naturally fractured reservoir. This method was able to describe the effects of fracture closure on the pressure fields due to the increasing effective compression stress. Thus, equivalent properties can be calculated like the permeability of the porous medium.

Acknowledgements

The authors wish to thank the financial support provided by CAPES (Coordenação de Aperfeiçoamento de Pessoal de Nível Superior) and CNPq (Conselho Nacional de Desenvolvimento Científico e Tecnológico).

REFERENCES

Abdelazim, R. and Rahman, S. S. (2016). Estimation of permeability of naturally fractured reservoirs by pressure transient analysis: An innovative reservoir characterization and flow simulation. *Journal of Petroleum Science and Engineering*, 145:404–422.

Barton, N., Bandis, S., and Bakhtar, K. (1985). Strength, deformation and conductivity coupling of rock joints. In *International Journal of Rock Mechanics and Mining Sciences & Geomechanics Abstracts*, volume 22, pages 121–140. Elsevier.

Cleto, P. R. (2016). Simulação de fraturamento hidráulico usando elementos finitos de elevada razão de aspecto com acoplamento hidromecânico. Master's thesis, Universidade Estadual Paulista.

Guimarães, L. (2002). *Análisis multi-componente no isotermo en medio poroso deformable no saturado*. PhD thesis, Universitat Politécnica de Catalunya.

Manzoli, O., Gamino, A., Rodrigues, E., and Claro, G. (2012). Modeling of interfaces in two-dimensional problems using solid finite elements with high aspect ratio. *Computers & Structures*, 94:70–82.

Manzoli, O., Maedo, M., Rodrigues, E., and Bittencourt, T. (2014). Modeling of multiple cracks in reinforced concrete members using solid finite elements with high aspect ratio. *Computational Modelling of Concrete Structures*, page 383.

Manzoli, O. L., Maedo, M. A., Jr., L. A. B., and Rodrigues, E. A. (2016). On the use of finite elements with a high aspect ratio for modeling cracks in quasi-brittle materials. *Engineering Fracture Mechanics*, 153:151 – 170.

Oliver, J., Huespe, A., Blanco, S., and Linero, D. (2006). Stability and robustness issues in numerical modeling of material failure with the strong discontinuity approach. *Computer Methods in Applied Mechanics and Engineering*, 195(52):7093 – 7114. Computational Modelling of Concrete.

Sánchez, M., Manzoli, O. L., and Guimarães, L. J. (2014). Modeling 3-d desiccation soil crack networks using a mesh fragmentation technique. *Computers and Geotechnics*, 62:27–39.

Seixas, M. G. (2015). *Modelagem Hidromecânica do Fraturamento Hidráulico de Rochas via Elementos Finitos com Elementos Especiais de Interface*. PhD thesis, Universidade Federal de Pernambuco.

Snow, D. T. (1965). *A parallel plate model of fractured permeable media*. PhD thesis, University of California.

Terzaghi, K. (1943). *Theoretical Soil Mechanics*. John Wiley and Sons, Inc.

Weng, X. (2015). Modeling of complex hydraulic fractures in naturally fractured formation. *Journal of Unconventional Oil and Gas Resources*, 9:114–135.